Proceedings of the
Annual Stability Conference
Structural Stability Research Council
Pittsburgh, Pennsylvania, May 10-14, 2011

On the Incorporation of Load Application Effects in the GBT Buckling Analysis of Thin-Walled Steel Beams and Frames

C. Basaglia, D. Camotim[1]

Abstract

This work deals with the development, finite element implementation and application of a Generalized Beam Theory (GBT) formulation intended to analyze the localized, local, distortional and global buckling behavior of thin-walled continuous beams and frames subjected to transverse loads applied at various member cross-section points (away from its shear centre). In order to take into account the effects stemming from the transverse load position, the GBT buckling formulation must incorporate geometrical stiffness terms stemming from either (i) the internal work of the pre-buckling transversal normal stresses ("exact" formulation) or (ii) the external work of the applied transverse loads (approximate/simplified formulation). After presenting the main concepts and procedures involved in the development of the above "exact" and simplified formulations, only the numerical implementation and application of the latter are addressed in the paper − although considerably easier, it provides fairly accurate results in most cases. The numerical results presented and discussed concern (i) hat-section cantilevers, (ii) two-span I-beams and (iii) I-section "L-frames", all acted by transverse loads applied at the top and bottom flanges, and make it possible to illustrate the capabilities (and also the limitations) of the proposed simplified formulation. The accuracy of the GBT-based results is assessed through the comparison with "exact" values, yielded by rigorous shell finite element analyses carried out in the code ANSYS.

1. Introduction

Due to their high global and local (wall) slenderness, the structural behavior of thin-walled open section steel members are invariably governed by localized (*e.g.*, web crippling), local, distortional and/or global instability phenomena. Therefore, the development, calibration and validation of design procedures and/or formulae for structures built from such members require the acquisition of in-depth knowledge about their buckling behavior, a task involving (i) the accurate evaluation of critical buckling stresses and (ii) the determination of the corresponding buckling mode shapes.

In practice, the members of any given slender steel structure are often subjected to loads applied at various cross-section locations – *e.g.*, beams acted by transverse loadings acting at the top flange. Even so, it seems fair to say that virtually all the information available on how the locations of the points of load application influence the member stability deals with global buckling, almost always beam lateral-

[1] Department of Civil Engineering and Architecture, ICIST/IST, Technical University of Lisbon, Lisbon, Portugal. cbasaglia@civil.ist.utl.pt and dcamotim@civil.ist.utl.pt

torsional buckling – aside from classical results included in books or manuals (*e.g.*, Trahair 1993), the works of Wang & Kitiporchai (1986), Mohri *et al.* (2003) and Andrade *et al.* (2007) deserve mention. As far as the local, distortional and localized buckling phenomena are concerned, the amount of research on the effects stemming from the transverse load position is still rather scarce. In this context, it is worth mentioning the works of (i) Gonçalves (2007), who used an approximate one-dimensional model to study the distortional buckling behavior of hat-section cantilevers acted by a tip point load, (ii) Samanta & Kumar (2006), who used shell finite element models to investigate the lateral-torsional-distortional buckling of singly symmetric I-section single-span beams acted by transverse loads applied at their top and bottom flanges, and (iii) Silva *et al*. (2008), who developed a GBT-based beam finite element to analyze rigorously (iii_1) problems involving localized buckling (*e.g.*, web crippling) and (iii_2) the effect of the point of load application in the local, distortional and global buckling behavior of isolated beams[2].

It should be mentioned that the use of shell finite element analysis to assess the buckling behavior of multi-span beams and frames is still prohibitive for routine application in design offices, since it involves a large modeling effort (including data input and result interpretation). A very promising alternative to this computer-intensive approach is the use of one-dimensional models (beam finite elements) based on Generalized Beam Theory (GBT). The authors have recently developed and numerically implemented GBT-based beam finite elements that make it possible to analyze the (elastic) local, distortional and global buckling behavior of continuous (multi-span) beams and frames (*e.g.*, Camotim *et al.* 2008, 2010a). However, such finite elements have two important limitations: they (i) can only be applied to thin-walled structural systems acted by transverse loads applied at the member shear centre axes and (ii) are not able to capture localized buckling phenomena (*e.g.*, web crippling).

The aim of this work is to overcome the above limitations, by developing, numerically implementing and illustrating the application of a GBT formulation that (i) takes into account the effects stemming from the transverse load position, with respect to the cross-section shear centre, and (ii) is capable of handling localized effects. This formulation must incorporate geometrical stiffness terms associated with either (i) the internal work of the pre-buckling transversal normal stresses ("exact" formulation) or (ii) the external work of the applied transverse loads (approximate/simplified formulation). After presenting the main concepts and procedures involved in the development of the above "exact" and simplified formulations, the paper addresses the numerical implementation and application of the latter[3] – although considerably easier, it still provides fairly accurate results in most cases (the exceptions are some web crippling problems). The numerical results presented and discussed concern (i) hat-section cantilevers, (ii) two-span I-beams and (iii) I-section "L-frames", all acted by top and bottom-flange transverse loads, and make it possible to illustrate the capabilities (and also the limitations) of the proposed simplified formulation. The accuracy of the GBT-based results is assessed through the comparison with "exact" values, yielded by rigorous shell finite element analyses carried out in the code ANSYS (SAS 2009).

2. Available GBT Formulations for Buckling Analysis

Consider the prismatic thin-walled member with the supposedly arbitrary open cross-section depicted in Fig. 1, where x, s, and z are local coordinates along the longitudinal direction (member axis), cross-section mid-line and wall thickness, which correspond the member mid-surface displacement components $u(x,s)$,

---

[2] Generalized Beam Theory (GBT) is a beam theory that incorporates genuine folded-plate concepts (*e.g.*, Schardt 1989 or Camotim *et al.* 2010b,c).

[3] Due to time limitations, it was not possible to implement numerically the "exact" GBT formulation developed at this time (it requires the performance of a rigorous GBT first-order analysis, which must include shear and transverse extension modes) – its numerical implementation, validation and illustration will be reported in the near future.

$v(x,s)$ and $w(x,s)$. The key GBT feature is the fact that these displacement components are expressed by means of a linear combination of cross-section deformation modes – *i.e.*, one has

$$u(x,s) = u_k(s)\phi_{k,x}(x) \qquad v(x,s) = v_k(s)\phi_k(x) \qquad w(x,s) = w_k(s)\phi_k(x) \quad , \quad (1)$$

where (i) $(.)_{,x} \equiv d(.)/dx$, (ii) the summation convention applies to subscript k, (iii) functions $u_k(s)$, $v_k(s)$, $w_k(s)$, yielded by a GBT cross-section analysis, characterize deformation mode k and (iv) $\phi_k(x) \equiv \phi_k(X)$ are mode amplitude functions defined along the member length (*e.g.*, Silvestre & Camotim 2003 or Gonçalves *et al.* 2009).

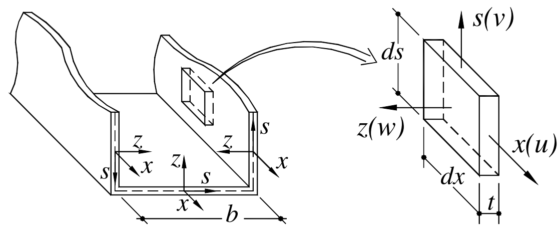

Figure 1: Prismatic thin-walled member with a supposedly arbitrary cross-section and infinitesimal wall element.

There are three GBT deformation mode families, namely (i) the conventional modes (those originally considered by Schardt (1989)), (ii) the (warping) shear modes and (iii) the transverse extension modes – the last two families were first introduced by Silvestre & Camotim (2003a)[4]. It is worth pointing out the following aspects, concerning the above deformation mode families:

(i) The conventional modes, which are based on the assumptions of null membrane shear strains and transverse extensions, constitute the core of GBT and can still be subdivided into (i_1) global modes (cross-section in-plane rigid-body motions: axial extension, major/minor axis bending and torsion), (i_2) distortional modes and (i_3) local modes. The last two mode subfamilies exhibit cross-section in-plane deformation (distortion and/or transverse wall bending), and only the torsion and distortional modes are associated with warping (longitudinal) displacements.

(ii) The shear modes stem from the non-linear variation of the warping displacements along the cross-section wall mid-lines. They involve exclusively warping displacements $u(s)$, *i.e.*, no membrane or flexural transverse displacements occur.

(iii) The transverse extension modes stem from the bowing effect associated with the transverse (local) bending of the cross-section walls. They only involve in-plane deformation (membrane and flexural transverse displacements), combined with null warping displacements ($u(s)=0$).

Once the deformation modes are known, one readily establishes and solves the member buckling eigenvalue problem. At this stage, it is worth pointing out that the participation of the non-conventional deformation modes in the buckling modes of steel members and frames is minute and can be disregarded without any loss in accuracy (*i.e.*, only the conventional deformation modes need to be included in a GBT buckling analysis)[5].

For quite a while, the performance of GBT buckling analyses was restricted to thin-walled members (and later also frames) subjected to uniform internal force and moment diagrams, a situation that was only

[4] For an in-depth discussion of the various types of deformation modes that can be identified and characterized by means of GBT cross-section analyses, the interested reader is referred to the recent work by Gonçalves *et al.* (2010).

[5] The same does not occur in FRP (fiber reinforced plastic) thin-walled members, characterized by quite low shear stiffness values. Thus, the critical buckling modes of such members often exhibit non-negligible participations from shear modes (*e.g.*, Silva *et al.* 2010) – excluding these modes from the GBT analyses may entail significant errors.

altered when Bebiano *et al.* (2007) developed a GBT formulation capable of analyzing single-span members subjected to non-uniform major and/or minor axis bending caused by transverse loadings. Recently, Basaglia *et al.* (2010) and Camotim *et al.* (2010a) extended this formulation to include non-uniform bimoment diagrams and, moreover, widened its domain of application to cover multi-span members, plane frames and space frames. However, this GBT formulation still had one fairly severe limitation: it could only accommodate transverse loads applied at the cross-section shear centre, which means that it could not capture the effects stemming from the load position w.r.t. shear centre – it has been well know for a long time that these effects are very relevant in the lateral-torsional buckling of beams (*e.g.*, *e.g.*, Trahair 1993), but there is very little knowledge on their influence on distortional or local buckling. Moreover, there was another (less severe) limitation: the inability to capture localized instabilities, like the web crippling phenomena that often occur in the webs of cross-section to highly concentrated transverse loads (patch loading).

In order to overcome the remaining limitations described in the previous paragraph, Silva *et al.* (2008a) proposed a GBT formulation to analyze isolated members subjected to transverse loadings applied away from the cross-section shear centre and able to capture localized buckling phenomena stemming from patch loading (*e.g.*, web crippling). However, this formulation (i) involves the performance of a rigorous GBT first-order (linear) analysis and (ii) is based on a novel approach to perform the GBT cross-section analysis that entails to the need to consider a rather large number of deformation modes (very fine cross-section discretization) (Silva *et al.* 2008b). This fact makes the application of the above formulation to multi-span members and/or frames (i) computationally very intensive (very large d.o.f. numbers are involved) and (ii) less "illuminating" (several deformation modes have no obvious structural meaning).

In view of the limitations/difficulties associated with the application of the above GBT formulation to multi-span members and/or frames, it was decided to propose an alternative approach – although based on several concepts and procedures previously developed, this approach also involves a number of novel features. For the benefit of the interested reader, the remainder of this section includes brief overviews of the GBT formulations developed by Bebiano *et al.* (2007)[6] and Silva *et al.* (2008a), naturally focusing on the features associated with the determination of the geometric stiffness (the key issue concerning the incorporation of the load application effects). Then, the next section will be devoted to the presentation of the GBT formulations proposed in this work – one "exact" and the other approximate/simplified.

2.1 GBT formulation developed by Bebiano et al. (2007)

The member equilibrium equations are obtained from the variational condition (equivalent to the Principle of Virtual Work)

$$\delta V = \delta U + \delta \Pi_{\sigma-x} + \delta \Pi_{\tau} = \int_{\Omega} \sigma_{ij} \delta\varepsilon_{ij} d\Omega + \int_{\Omega} \sigma^{0}_{xx} \delta\varepsilon_{xx} d\Omega + \int_{\Omega} \tau^{0}_{xs} \delta\gamma_{xs} d\Omega = 0 \quad , \quad (2)$$

where (i) Ω is the structural system volume (*n* plates), (ii) δU is the first variation of the strain energy, given by the tensor product between the internal stresses σ_{ij} ($\sigma_{xs} \equiv \tau_{xs}$) and strain variations $\delta\varepsilon_{ij}$ ($\delta\varepsilon_{xs} \equiv \delta\gamma_{xs}$) associated with the buckling action/mode, and (iii) $\delta\Pi_{\sigma-x}$ and $\delta\Pi_{\tau}$ are the works done by the pre-buckling longitudinal normal (σ^{0}_{xx}) and shear (τ^{0}_{xs}) stresses, deemed constant with their final values and statically equivalent to the (longitudinally varying) internal forces, moments and bimoments, over the strain variations $\delta\varepsilon_{ij}$. Note that the sum of $\delta\Pi_{\sigma-x}$ and $\delta\Pi_{\tau}$ can also be viewed as the work done by the applied loads and/or moments over the displacement variations associated with the buckling action/mode.

[6] Including also the modification/extension carried out by Basaglia *et al.* (2010) and Camotim *et al.* (2010a).

Since Bebiano *et al.* (2007) adopted the usual GBT simplifying assumption of null membrane linear shear strains ($\gamma_{xs}^{M.L}=0$), the pre-buckling shear stresses τ_{xs}^{0} cannot be evaluated through the member (plane stress) constitutive relations. Instead, the authors resorted to the longitudinal stress equilibrium equations from of classical beam theory to obtain τ_{xs}^{0} (balance between pre-buckling longitudinal normal stress gradients and shear stresses). However, since this formulation also assumes null membrane transverse extensions ($\varepsilon_{ss}^{M}=0$), it can only handle only members with doubly symmetric cross-sections (coincident centroid and shear centre). Then, the variational form of the equilibrium conditions involves only conventional modes and reads (L is the member length)

$$\delta V=\int_L\Big(C_{ik}\phi_{k,xx}\delta\phi_{i,xx}+D_{ik}^{1}\phi_{k,x}\delta\phi_{i,x}+D_{ik}^{2}\phi_{k}\delta\phi_{i,xx}+D_{ki}^{2}\phi_{k,xx}\delta\phi_{i}+B_{ik}\phi_{k}\delta\phi_{i}+$$
$$+\lambda\,[W_j^0X_{jik}^{\sigma-x}\phi_{k,x}\delta\phi_{i,x}-W_{j,x}^0X_{jik}^{\tau}(\phi_i\delta\phi_{k,x}+\phi_{k,x}\delta\phi_i)]\Big)dx=0\qquad W_j^0=C_{jj}\phi_{j,xx}^0\quad,\quad(3)$$

where (i) C_{ik}, D_{ik}^{1}, D_{ik}^{2} and B_{ik} are second-order tensors providing the member linear stiffness, (ii) λ is the load parameter and (iii) $X_{jik}^{\sigma-x}$ and X_{jik}^{τ} are the geometric stiffness tensors stemming from the pre-buckling longitudinal normal stresses σ_{xx}^{0} (W_1^0, W_2^0, W_3^0 and W_4^0 concern the compressive axial force, major/minor axis bending moment and bimoment) and shear stresses τ_{xs}^{0} (major/minor axis bending moment and bimoment gradients – minor/major axis shear and bishear) Their components are given by (E, υ and G are the material Young's modulus, Poisson's ratio and shear modulus)

$$C_{ik}=E\int_b t\,u_iu_k ds+\frac{E}{12(1-\upsilon^2)}\int_b t^3\,w_iw_k ds\qquad B_{ik}=\frac{E}{12(1-\upsilon^2)}\int_b t^3\,w_{i,ss}w_{k,ss}ds$$

$$D_{ik}^{1}=\frac{G}{3}\int_b t^3\,w_{i,s}w_{k,s}ds\qquad D_{ik}^{2}=\frac{\upsilon E}{12(1-\upsilon^2)}\int_b t^3\,w_iw_{k,ss}ds\quad,\quad(4)$$

$$X_{jik}^{\sigma-x}=\frac{E}{C_{jj}}\int_b t\,u_j(v_iv_k+w_iw_k)ds\;{}^{7}\qquad X_{jik}^{\tau}=\frac{E}{C_{jj}}\int_b F_j(s)\,w_{i,s}w_k ds\quad,\quad(5)$$

where F_j(s) is the first moment of (i) a cross-section zone, with respect to the major/minor axis ($j=2$ or 3), or of (ii) a sectorial area zone, with respect to the shear centre ($j=4$).

2.2 GBT formulation developed by Silva et al. (2008a)

The member equilibrium equations are now enhanced with the inclusion of a geometric stiffness term stemming from the transverse normal stresses ($\delta\overline{\Pi}_{\sigma-s}$). The corresponding variational condition is

$$\delta\overline{V}=\delta\overline{U}+\delta\overline{\Pi}_{\sigma-x}+\delta\overline{\Pi}_{\tau}+\delta\overline{\Pi}_{\sigma-s}=0\quad,\quad(6)$$

where the new term stands for the work done by the applied transverse normal stresses σ_{ss}^{0} over the strain variations $\delta\varepsilon_{ij}$ – this work is null when the transverse loads are applied at the cross-section shear centre. Moreover, Silva *et al.* (2008a) proposed a novel methodology to evaluate the geometric stiffness terms, which (i) is based on the deformation modes determined by means of the novel GBT cross-section analysis proposed in Silva *et al.* (2008b) and (ii) involves the following steps:

(i) Perform a rigorous first-order (geometrically non-linear) GBT analysis of the member subjected to a reference loading (to be multiplied by the load parameter λ in the buckling analysis). This analysis

[7] The component $X_{244}^{\sigma-x}$ proposed by Bebiano *et al.* (2007) is not applicable to transversally loaded beams with cross-sections that are not symmetric with respect to the major axis. If this is the case, $X_{244}^{\sigma-x}$ must be corrected with the addition of a term consisting of the shear centre coordinate, along the minor axis, with respect to cross-section centroid (z_C).

must include all deformation modes (which cover the space spanned by the conventional, shear and transverse extension modes characterized earlier, but do not necessarily coincide with them) and its output are the member longitudinal normal, transverse normal and shear stress distributions.

(ii) Compute the geometric stiffness tensors associated with the stress distributions obtained in the previous item, which are written in terms of deformation mode amplitudes and their derivatives.

(iii) Establish the buckling problem defined in (6), which involves

$$\delta\overline{U} = \int_L (\overline{C}_{ik}\phi_{k,xx}\delta\phi_{i,xx} + \overline{D}^1_{ik}\phi_{k,x}\delta\phi_{i,x} + \overline{D}^2_{ik}\phi_k\delta\phi_{i,xx} + \overline{D}^2_{ki}\phi_{k,xx}\delta\phi_i + \overline{B}_{ik}\phi_k\delta\phi_i)dx \tag{7}$$

$$\delta\overline{\Pi}_{\sigma-x} = \lambda\int_L (\overline{X}^{\sigma-x}_{jik}\phi^0_{j,xx}\phi_{k,x}\delta\phi_{i,x})dx \qquad \delta\overline{\Pi}_{\sigma-s} = \lambda\int_L (\overline{X}^{\sigma-s}_{jik}\phi^0_j\phi_k\delta\phi_i)dx$$

$$\delta\overline{\Pi}_{\tau} = \lambda\int_L (\overline{X}^{\tau}_{jik}\phi^0_{j,x}\phi_{k,x}\delta\phi_i + \overline{X}^{\tau}_{jki}\phi^0_{j,x}\phi_i\delta\phi_{k,x})dx \quad , \tag{8}$$

where (iii[1]) the second-order tensors $\overline{C}_{ik}$, $\overline{B}_{ik}$, $\overline{D}^1_{ik}$ and $\overline{D}^2_{ik}$ account for the linear stiffness values associated with longitudinal extensions, transverse extensions, shear strains and coupling between longitudinal and transverse extensions (Poisson effects), respectively, and (iii[2]) the third-order tensors $\overline{X}^{\sigma-x}_{jik}$, $\overline{X}^{\sigma-s}_{jik}$ and $\overline{X}^{\tau}_{jik}$, included in the geometric stiffness terms, concern the works done by the longitudinal normal, transverse normal and shear stresses over the variations of the non-linear longitudinal extensions ($\varepsilon^{NL}_{xx} = (v^2_{,x} + w^2_{,x})/2$, transverse extensions ($\varepsilon^{NL}_{ss} = w^2_{,s}/2$) and shear strains ($\gamma^{NL}_{ss} = w_{,x}w_{,s}$). The components of these second and third-order tensors are given by

$$\overline{C}_{ik} = \frac{E}{1-\upsilon^2}\int_b t\,u_i u_k ds + \frac{E}{12(1-\upsilon^2)}\int_b t^3\, w_i w_k ds \qquad \overline{B}_{ik} = \frac{E}{1-\upsilon^2}\int_b t\,v_{i,s}v_{k,s} ds + \frac{E}{12(1-\upsilon^2)}\int_b t^3\, w_{i,ss}w_{k,ss} ds$$

$$\overline{D}^1_{ik} = G\int_b t\,(u_{i,s}+v_i).(u_{k,s}+v_k)ds + \frac{G}{3}\int_b t^3\, w_{i,s}w_{k,s} ds$$

$$\overline{D}^2_{ik} = \frac{\upsilon E}{1-\upsilon^2}\int_b t\,u_i v_{k,s} ds + \frac{\upsilon E}{12(1-\upsilon^2)}\int_b t^3\, w_i w_{k,ss} ds \tag{9a}$$

$$\overline{X}^{\sigma-x}_{jik} = \frac{E}{1-\upsilon^2}\int_b t\,u_j(v_i v_k + w_i w_k)ds \qquad \overline{X}^{\sigma-s}_{jik} = \frac{E}{1-\upsilon^2}\int_b t\,v_{j,s}w_{i,s}w_{k,s} ds$$

$$\overline{X}^{\tau}_{jik} = G\int_b (u_{j,s}+v_j)\,w_{i,s}w_k ds \quad . \tag{9b}$$

(iv) Solve the above buckling problem by means of a GBT-based beam finite element implementation similar to that originally developed by Silvestre & Camotim (2003b), in the context of the buckling analysis of pultruded FRP members.

Since this formulation is based on a cross-section discretization that does not lead to the conventional, shear and transverse extension deformation modes proposed by Silvestre & Camotim (2003a) (even if the deformation space spanned by them is fully covered), accurate buckling results can only be consistently achieved by including all deformation modes in the analysis – several of them with no obvious structural meaning. As mentioned earlier, this feature (i) makes the application to multi-span members and/or frames computationally very intensive and (ii) clouds the structural interpretation of the results obtained.

3. Proposed GBT Formulations

The GBT formulations for buckling analysis proposed in this section are devised to overcome the above limitations/difficulties, while still being able to adequately (i) account for the effects due to the transverse load position, with respect to the cross-section shear centre, and (ii) capture localized buckling phenomena. The first of them, termed "exact", only differs from the one developed by Silva *et al.* (2008a) in the fact that it is based on the "traditional" GBT cross-section analysis/discretization, due to Silvestre & Camotim (2003a) – instead of adopting the novel approach proposed by Silva *et al.* (2008b). The main advantages of using the "traditional" GBT deformation mode families are (i) a considerable reduction in the number of d.o.f. involved in performing a buckling analysis (a non-negligible aspect in multi-span members and frames), without sacrificing the accuracy of the results obtained, and (ii) retaining the "structural clarity" that characterizes (is trademark of) the GBT analyses.

Due to time limitations, it has not yet been possible to carry out the numerical (beam finite element) implementation and illustration of the "exact" GBT formulation mentioned in the previous paragraph. Instead, one presents in this work the development of an approximate/simplified alternative formulation that is much easier to implement numerically. Indeed, it consists of enhancing the GBT formulation developed by Bebiano *et al.* (2007) through the inclusion of a term providing an approximate (but fairly accurate in most cases) estimate of the work done by the applied transverse loads – this term accounts for the geometric stiffness associated with the transverse normal stresses.

3.1 "Exact" formulation

As mentioned earlier, this formulation is fairly similar to that developed by Silva *et al.* (2008a). The key difference resides in the adoption of the GBT cross-section analysis/discretization developed by Silvestre & Camotim (2003a) adopted, which also entails a few additional modifications. The most relevant concepts and procedures involved in the application and implementation (yet to be done) of this "exact" formulation main are briefly described next:

(i) Perform a rigorous GBT-based (beam finite element) first-order analysis, defined by

$$\mathbf{d}^{0} = \mathbf{K}^{-1}\mathbf{f}^{0} \quad , \quad (10)$$

where (i) $\mathbf{K}$ is the member or frame linear stiffness matrix, and (ii) $\mathbf{f}^0$ is the applied load vector, expressed in modal form, and (iii) $\mathbf{d^0}$ is the pre-buckling generalized displacement vector, also expressed in modal form. Since the objective of this first-order analysis is to determine accurately the pre-buckling longitudinal normal, transverse normal and shear stress distributions, it must include conventional, transverse extension and shear deformation modes. However, unlike in the approach proposed by Silva *et al.* (2008a), not all of these modes need to be considered in most cases. Indeed, previous studies by Basaglia *et al.* (2008), carried out in the context of GBT post-buckling analysis, provided a firm evidence that the inclusion of *2-3* shear and/or transverse extension modes in the member/frame GBT first-order analysis suffices to obtain practically "exact" pre-buckling transverse normal and shear stress distributions – at least for cross-sections without "too many walls", such as I, hat, zed, channel or rack-sections.

(ii) Compute the geometric stiffness tensors associated with (ii_1) the three stress distributions obtained in the previous item, which are written in terms of the amplitudes and respective derivatives of the deformation modes included in the first-order analysis, and (ii_2) the deformation modes to be included in the buckling analysis – in steel members and frames (those dealt with in this work), only a fraction of the conventional modes is necessary to achieve accurate buckling loads and mode shapes.

(iii) Establish and solve, by means of GBT-based beam finite elements, the buckling problem defined by eqs. (6)-(8), where (iii$_1$) $\delta\overline{U}$ includes only contributions from the conventional modes considered in the buckling analysis, and (iii$_2$) indices in $\delta\overline{\Pi}_{\sigma-x}$, $\delta\overline{\Pi}_{\tau}$ and $\delta\overline{\Pi}_{\sigma-s}$ concern the deformation modes used to obtain the pre-buckling stress distributions (j) and included in the buckling analysis (i and k).

(iv) At this stage, it is worth noting that the number of d.o.f. (deformation modes) involved in performing a GBT buckling analysis according to this approach is much smaller than that required by the application of the methodology prescribed by Silva *et al.* (2008a). Indeed, the latter stipulates that all deformation modes stemming from the cross-section discretization must be included in both the GBT first-order and buckling analyses – all the indices appearing in eqs. (7)-(8), namely i, j and k, span the whole deformation space. This considerable d.o.f. reduction, the main advantage of this "exact" GBT formulation, makes its application to multi-span members and frames much more appealing (and viable) in computational terms.

3.2 Approximate/simplified formulation

An interesting alternative to the above "exact" GBT formulation is the approximate/simplified approach presented next. It consists of enhancing the formulation developed by Bebiano *et al.* (2007)[8], which was developed to capture the effects stemming from the longitudinal normal stress gradients and the ensuing shear stresses, through the inclusion of the additional geometrical stiffness due to the transverse load application effects. One distinctive advantage of this approach is the fact that it does not require the performance of a first-order analysis (to obtain the pre-buckling stress distributions) and involves only the consideration of the conventional deformation modes. Indeed, the load application effects are taken into account through the works done by these loads over the displacement variations associated with the deformation modes participating in the buckling mode (which vary from case to case). These works are calculated by means of kinematical models based on the deformation patterns of the deformation modes contributing to the buckling mode – an approach similar to that adopted in classical beam theory to assess the influence of the transverse load position on lateral-torsional buckling (*e.g.*, Trahair 1993).

Without any loss of generality, the implementation of the approximate/simplified approach is illustrated by means of the mono-symmetric hat-section beam depicted in Fig. 2. Let x, y and z denote the beam longitudinal axis and the cross-section major and minor principal axes, respectively. The origin of y and z is the cross-section centroid G, which does not coincide with the shear centre C (its coordinates are $y_C=0$ and z_C). The beam is subject to (i) two uniformly distributed loads $q_z/2$, applied along the top web-flange longitudinal edges (P_L and P_R axes, located e_{z1} below the shear centre) and (ii) two mid-span point loads $Q_z/2$, applied at the web-stiffener corners (points R_L and R_R, located e_{z2} below the shear centre).

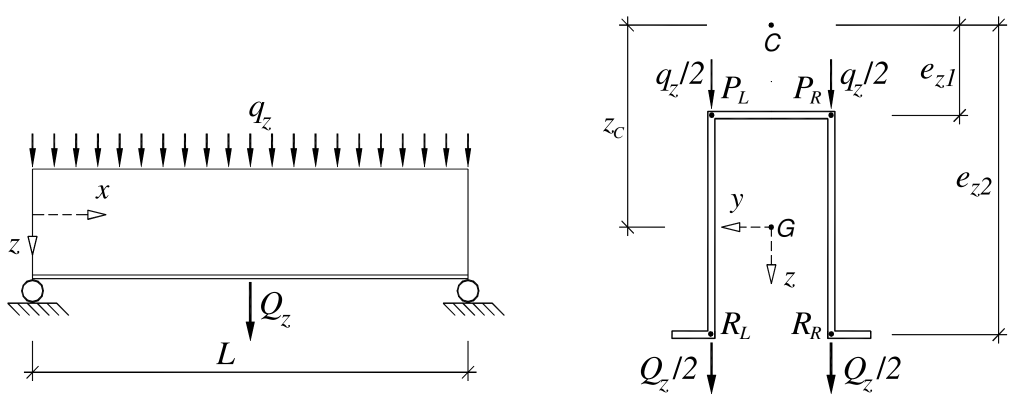

Figure 2: Illustrative mono-symmetric hat-section beam: geometry and loading.

[8] As modified/extended by Basaglia *et al.* (2010) and Camotim *et al.* (2010a), including the addition of the z_C term to $X_{244}^{\sigma-x}$.

The (external) work done by the four applied loads (Π) is given by

$$\Pi = \frac{q_z}{2}\int_L [\, w_{PL}(x) + w_{PR}(x) \,] dx + \frac{Q_z}{2}[\, w_{RL} + w_{RR} \,] \quad , \quad (11)$$

where $w_{PL}(x)$, $w_{PL}(x)$, w_{RL} and w_{RR} are the vertical displacements of the top web-flange longitudinal edges and mid-span point web-stiffener corners. Excluding the pre-buckling displacements (major axis bending – cross-section rigid-body translations along z), whose influence on the beam buckling behavior is disregarded (linear buckling analysis), the above displacements may have contributions from the GBT (i) torsion, (ii) distortional and (iii) local deformation modes. The in-plane deformed shapes of some of these modes are depicted in Fig. 3 and the contributions from modes **4** (torsion), **5** (distortional) and **7** (local) are addressed individually next – those from the remaining distortional and local modes are similar.

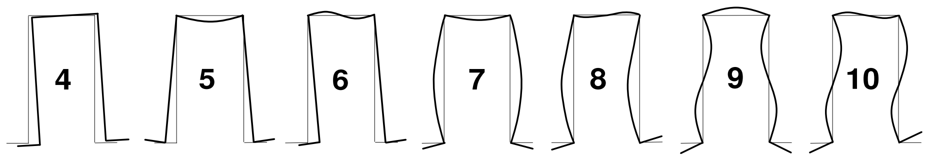

Figure 3: Torsion (**4**), Distortional (**5**-**6**) and local (**6**-**10**) hat-section deformation modes.

(I) *Torsion Deformation Mode* (**4**). As shown in Fig. 4, the displacements $w_{PL.4}(x)$, $w_{PR.4}(x)$, w_{RL4} and $w_{RR.4}$ correspond to the vertical displacements of (i) axes P_L and P_R and (ii) points R_L and R_R caused by the torsional rotation, which are given by (positive downwards)

$$w_{PL.4} \approx \frac{b_f}{2}\sin w_{4,s} - \frac{e_{z1}\, w_{4,s}^2}{2} \qquad w_{PR.4} \approx -\frac{b_f}{2}\sin w_{4,s} - \frac{e_{z1}\, w_{4,s}^2}{2}$$

$$w_{RL.4} \approx \frac{b_f}{2}\sin w_{4,s} - \frac{e_{z2}\, w_{4,s}^2}{2} \qquad w_{RR.4} \approx -\frac{b_f}{2}\sin w_{4,s} - \frac{e_{z2}\, w_{4,s}^2}{2} \quad , \quad (12)$$

where b_f is flange width and $w_{4,s}$ is the cross-section rigid-body torsional rotation.

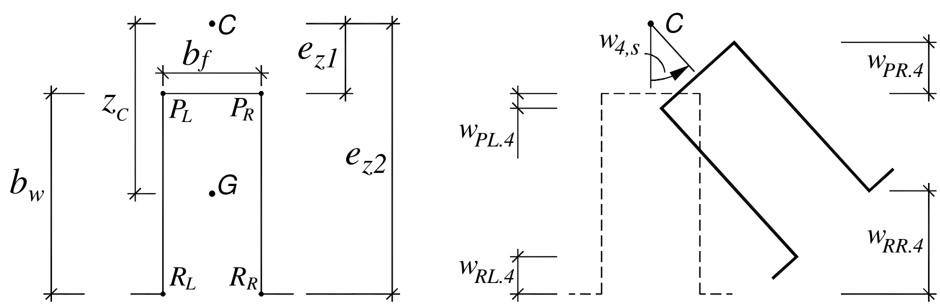

Figure 4: Hat-section geometry and vertical displacements caused by the torsion mode.

(II) *Distortional Deformation Mode* (**5**). In the context of the simplified model adopted here, the vertical displacements caused by this symmetric distortional mode stem exclusively from the rigid-body rotations of the vertical webs about their top ends[9]. Therefore, one has (see Fig. 5)

$$w_{PL.5} = w_{PR.5} = 0 \qquad w_{RL.5} = w_{RR.5} \approx -\frac{b_w\,(w_{5,s})^2}{2} \quad , \quad (13)$$

where b_w is width/height of the webs and $w_{5,s}$ stands for their common rigid-body rotation.

[9] Note that, for a transverse load was applied at the horizontal flange mid-point, the vertical displacement would stem exclusively from the flange transverse bending.

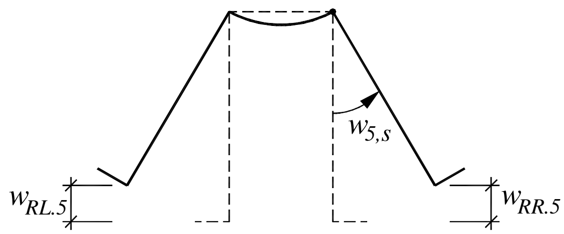

Figure 5: Vertical displacements caused by the distortional mode **5**.

(III) *Local Deformation Mode* (**7**). The displacements $w_{PL7}(x)$, $w_{PR.7}(x)$, $w_{RL.7}$ and $w_{RR.7}$ are bounded by the vertical shortening of the left and right webs caused by their transverse bending associated with this symmetric local mode – see Fig. 6(a). The value of this vertical shortening Δ is given by

$$\Delta = \frac{1}{2}\int_{0}^{b_w}(w_{7,s})^2\,ds \qquad . \quad (14)$$

Since it is not possible to determine the vertical displacements of the cross-section corners where the loads are applied (in the "exact" formulation, the corresponding work term is evaluated on the basis of the transverse normal stresses obtained from a GBT first-order analysis), the following simplifying assumption was adopted: (i) to view the webs as simply supported columns under a combination of compression and tension[10] and (ii) to partition Δ according to their compressed and tensioned zones – the shortenings of the compressed and tensioned web heights "count" as positive (downwards) and negative (upwards), respectively. According to this simplifying assumption, the displacements of the loads applied at the top and bottom web ends are given by, respectively,

$$w_{PL.7} = w_{PR.7} \approx \frac{1}{2}\int_{0}^{b_w}(w_{7,s})^2\,ds \qquad\qquad w_{RL.7} = w_{RR.7} \approx -\frac{1}{2}\int_{0}^{b_w}(w_{7,s})^2\,ds \qquad . \quad (15)$$

Fig. 6(b) shows the models associated with the determination of these displacement values.

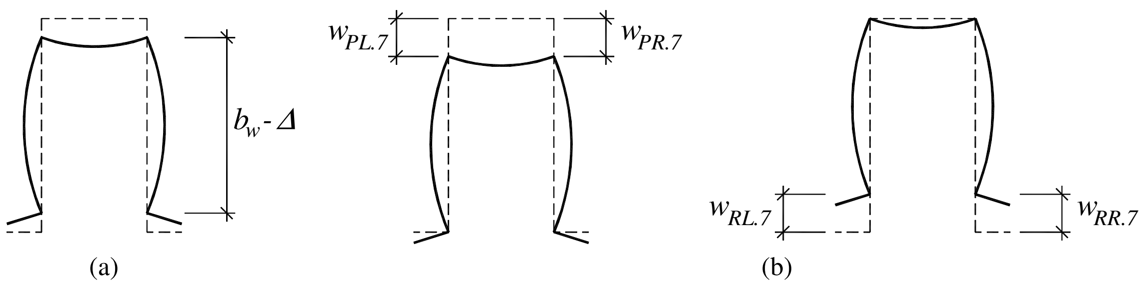

Figure 6: (a) Web vertical shortening and (b) vertical displacements (top and bottom loading) attributed to local mode **7**.

The geometric stiffness $\delta\overline{\Pi}_{\sigma-s}$, appearing in (6) and defined in (8) on the basis of pre-buckling transverse normal stresses, is then replaced by the first variation of the work done by the applied transverse loads ($\delta\Pi$). Denoting by q_0 and Q_0 the load reference values, which must correspond to ϕ_j^0 in eq. (8), it reads

$$\delta\Pi = \lambda\frac{q_0}{2}\int_{L}[\,w_{PL,x} + w_{PR,x}\,]dx + \lambda\frac{Q_0}{2}[\,w_{RL,x} + w_{RR,x}\,] \qquad . \quad (16)$$

---

[10] The cases of top and bottom (downward) loading correspond to full compression and full tension, respectively. If the load was applied within the web height, its upper and lower zones would be under tension and compression, respectively.

This term must be added to eq. (2), which thus becomes

$$\delta V = \delta U + \delta \Pi_{\sigma-x} + \delta \Pi_{\tau} + \delta \Pi_{\sigma-s} = 0 \quad , \quad (17)$$

where $\delta\Pi_{\sigma-s}$ must be expressed in modal form, individualizing the contributions of all the relevant deformation modes (torsion, distortional and/or local). If only modes **4**, **5** and **7** (those addressed earlier) were relevant, the additional term would be given by

$$\begin{aligned} \delta \Pi_{\sigma-s} = {} & \lambda q_0 \left(-\int_L e_{z1} w_{4,s}^2 \phi_4 \delta\phi_4 \, dx + \int_L \int_0^{b_w} w_{7,s}^2 \phi_7 \delta\phi_7 \, ds dx \right) + \\ & + \lambda Q_0 \left(- e_{z2} w_{4,s}^2 \phi_4 \delta\phi_4 - b_w w_{5,s}^2 \phi_5 \delta\phi_5 - \int_0^{b_w} w_{7,s}^2 \phi_7 \delta\phi_7 \, ds \right) \end{aligned} \quad . \quad (18)$$

Finally, the solution of (17), involving only conventional deformation modes, can be obtained by means of the GBT based beam finite elements developed by (i) Camotim *et al.* (2008), for continuous beams, and by (ii) Camotim *et al.* (2010a), for frames: 2-node elements and linear combinations of Hermite cubic polynomials to approximate the modal amplitude functions $\phi_k(x)$.

4. Illustrative Examples

In order to illustrate the application, capabilities and limitations of the proposed approximate/simplified GBT formulation, three sets of numerical results are presented and discussed in this section. They concern the local, distortional, global and localized buckling behavior of (i) hat-section cantilevers, (ii) two-span I-beams and (iii) I-section "L-frames", all acted by transverse loads applied at two different locations. The GBT-based results are compared with values yielded by rigorous ANSYS (SAS 2009) shell finite element analyses – members/frames discretized into fine meshes of SHELL181 elements (ANSYS nomenclature).

Fig. 7 shows the cross-section geometries (shapes and dimensions) and adopted GBT discretizations of the thin-walled steel members dealt with in this work. Figs. 8 and 9 depict the in-plane deformed configurations of the most relevant deformation modes (*i.e.*, those with significant contributions to the buckling modes of the members and frames dealt with in this work).

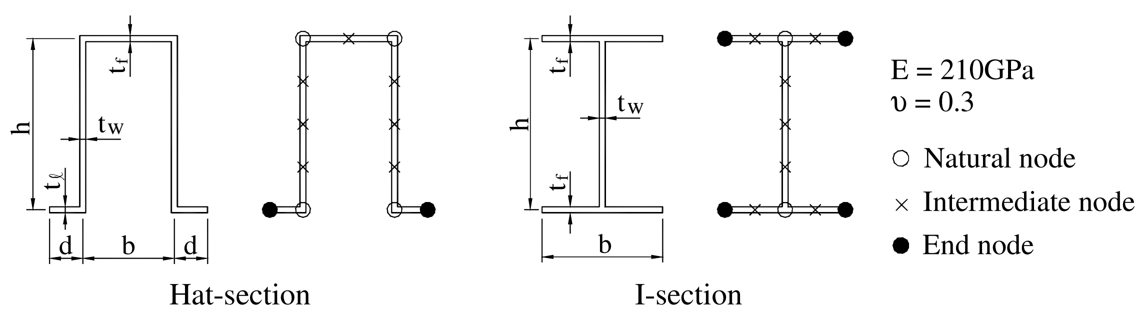

Designation	Shape	Web h (mm)	Flange b (mm)	Lip d (mm)	Thickness t_w (mm)	Thickness t_f (mm)	Thickness t_ℓ (mm)
HS120×60	Hat-section	120	60	20	2.0	2.0	2.0
I300×150	I-section	300	150	–	4.75	6.35	–
I300×200		300	200	–	5.0	5.0	–

Figure 7: Hat-section and I-section dimensions and adopted GBT discretizations.

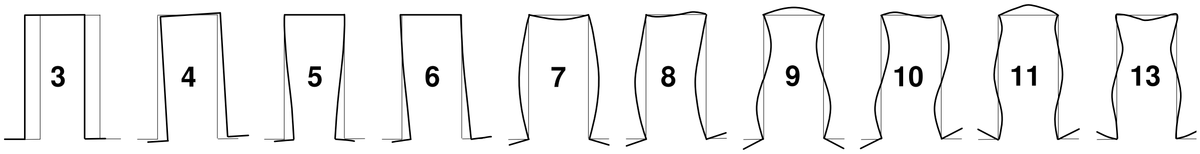

Figure 8: In-plane deformed configurations of the most relevant hat-section deformation modes.

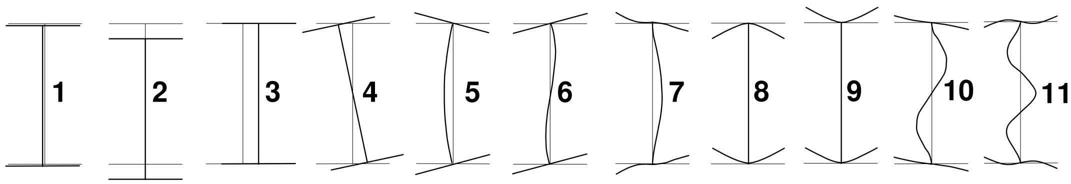

Figure 9: In-plane deformed configurations of the most relevant I-section deformation modes.

4.1 Hat-section cantilevers

One analyses the buckling behavior of HS120×60 cantilevers of lengths *L=25*, *50*, *100* and *200cm* and acted by two identical transverse point loads applied at either the free-end web-flange or web-stiffener corners (top and bottom tip loading). The main objective is to assess the influence of the load position on the cantilever critical buckling load and mode shape. While Table 1 shows the GBT and ANSYS critical loads corresponding to the four lengths and the two loadings, Figs. 10 and 11 provide two buckling mode representations: (i) ANSYS 3D views and (ii) GBT modal amplitude functions $\phi_k(x)$. The observation of these buckling results prompts the following remarks:

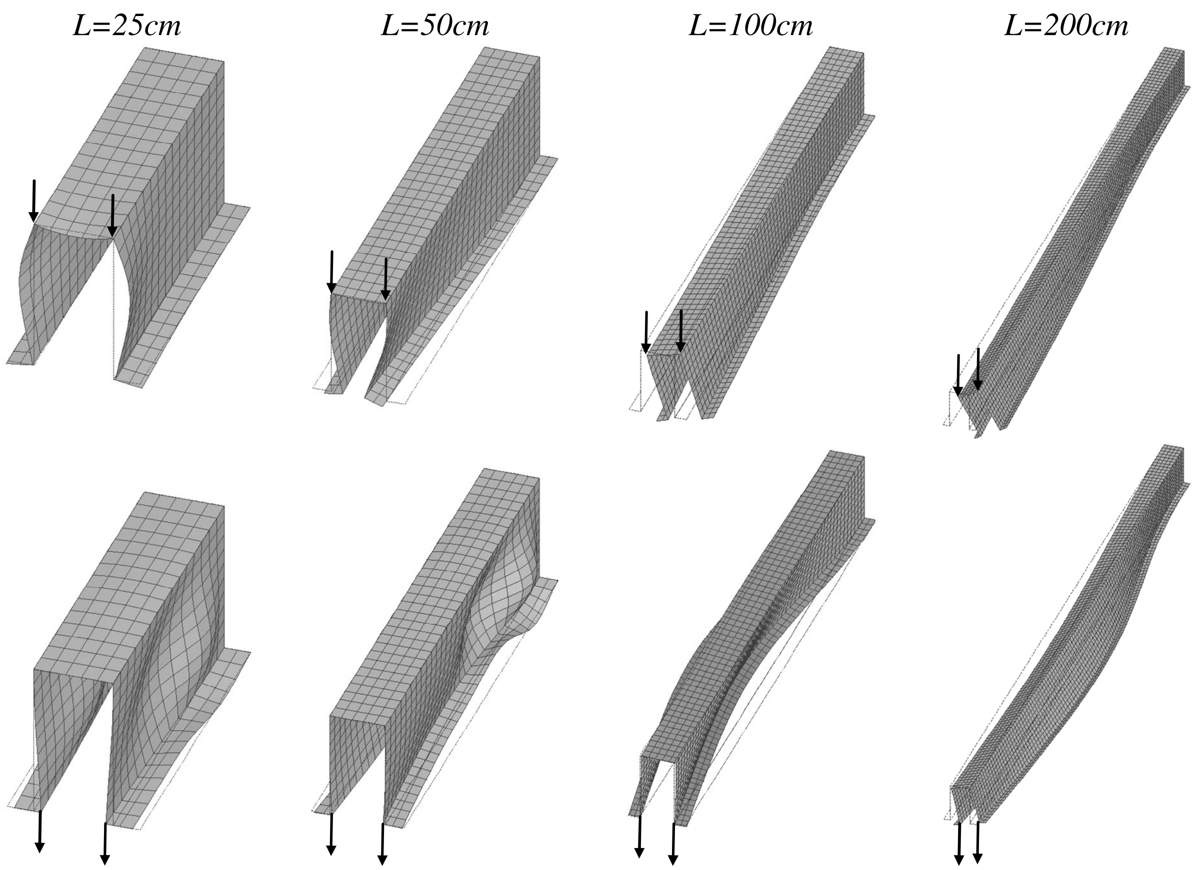

Figure 10: ANSYS critical buckling mode shapes for the four cantilever lengths and two loadings under consideration.

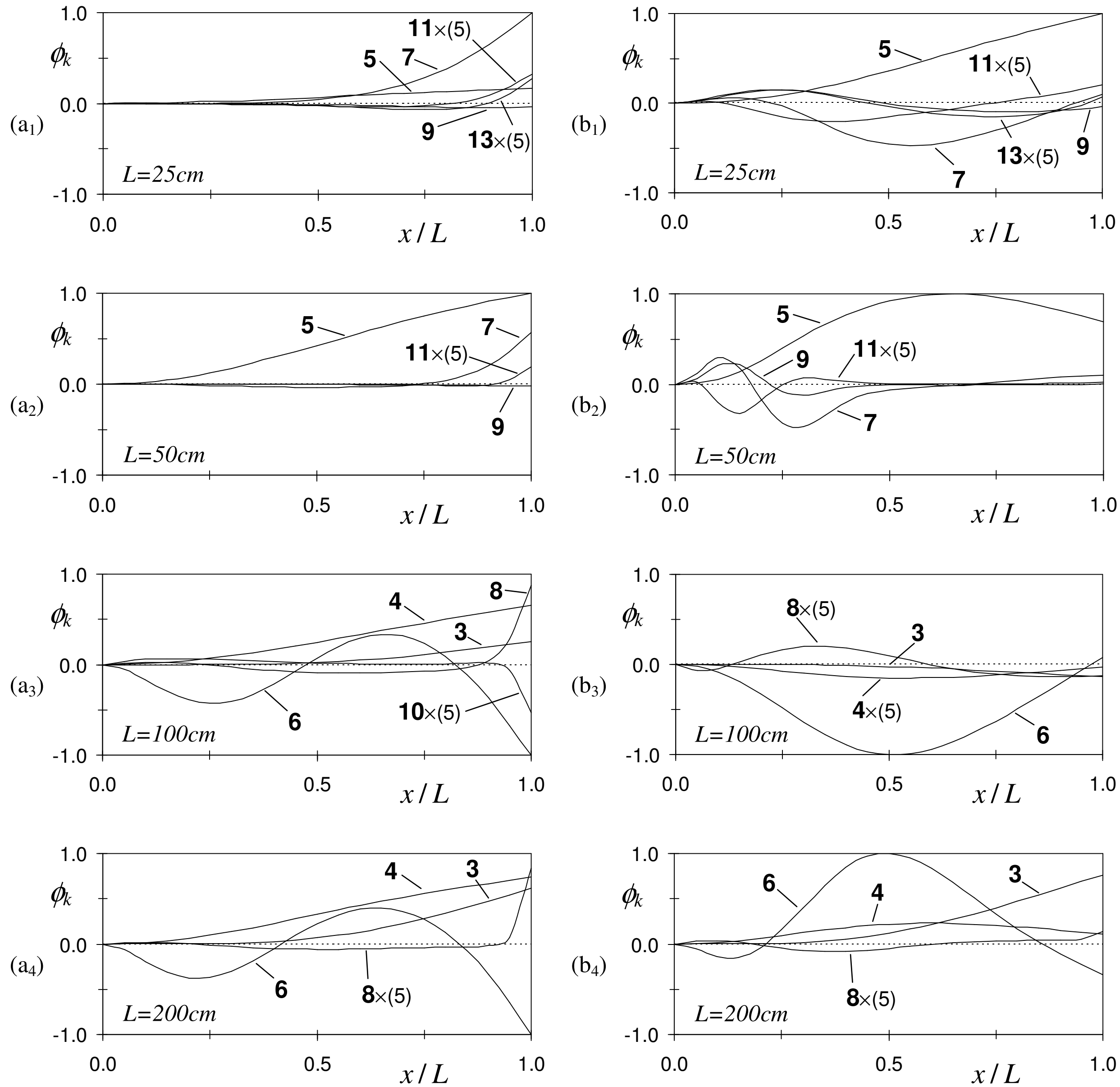

Figure 11: Mode amplitude functions of cantilevers with four lengths under (a_1–a_4) top and (b_1–b_4) bottom loading.

Table 1: GBT and ANSYS cantilever critical load values (kN).

Length (*cm*)	*25*		*50*		*100*		*200*	
Load application	*Top*	*Bottom*	*Top*	*Bottom*	*Top*	*Bottom*	*Top*	*Bottom*
GBT	31.74	104.72	26.46	55.08	11.27	15.44	2.15	3.52
ANSYS	34.60	99.99	28.97	51.91	10.85	15.30	2.11	3.43
Δ (%)	-8.3	4.7	-8.7	6.1	3.9	0.9	1.9	2.6

(i) There is a clear difference between the critical buckling loads and mode shapes associated with top and bottom loading. Concerning the critical loads, those corresponding to bottom loading may exceed their top loading counterparts by over *280%* (*L=25cm*). In either case, the critical buckling modes exhibit relevant contributions from global, distortional and local deformation modes.

(ii) In the shorter cantilevers (*L=25*;*50cm*) buckling is clearly triggered by the web localized instability and combine symmetric distortional (**5**) and local (**7**, **9**, **11**, **13**) deformation modes. On the other hand, the longer cantilever (*L=100*;*200cm*) buckling modes involve anti-symmetric global (**3**, **4**), distortional (**6**) and local (**8**, **10**) deformation modes.

(iii) The maximum deformations occur (iii_1) in the free end region, for the top loading buckling modes, and (iii_2) in the vicinity of the support and at mid-length, for the bottom loading buckling modes.

(iv) The two critical buckling mode representations shown in Figs. 10 and 11 agree quite closely.

(v) The GBT and ANSYS critical loads are very close for *L=100*;*200cm* – differences below *4%* (all overestimations). For *L=25*;*50cm*, the GBT and ANSYS values differ by *8.3%* and *8.7%* (top loading – underestimations) and by *4.7%* and *6.1%* (bottom loading – overestimations).

(vi) The discrepancy between the GBT and ANSYS short cantilever critical loads is clearly due to the (expected) inaccuracy in capturing the influence of the load point of application on the geometric stiffness associated with the local deformation modes. Indeed, while the approximated/simplified model adopted assumes, in this case, uniform compressive (top loading) and tensile (bottom loading) pre-buckling web transverse normal stresses, the real stress distributions are far from uniform – *e.g.*, see those concerning the *L=25cm* cantilevers, depicted in Fig. 12. Since the "exact" formulation (not yet implemented) should be able to capture these non-uniform stress distributions quite accurately, it seems fair to anticipate that it will lead to much more accurate short cantilever critical buckling loads.

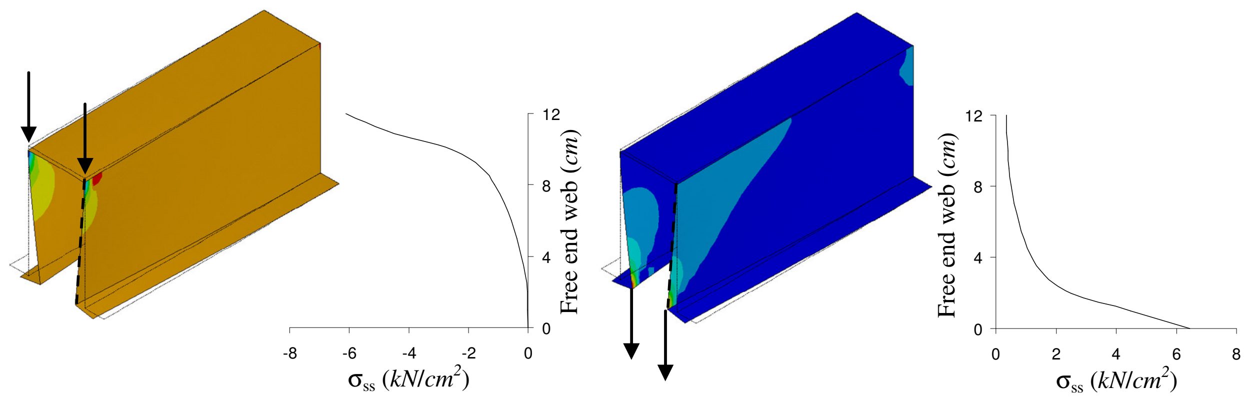

Figure 12: *L=25cm* cantilever pre-buckling transverse normal stresses for top and bottom loading (ANSYS results).

4.2 Two-span I-beams

Next, one investigates the buckling behavior of two-span symmetric beams with (i) overall length *L=400cm* (*2×200cm*) or *L=800cm* (*2×400cm*) and (ii) I300×150 cross-sections. They are acted by two identical mid-span transverse point loads, applied at either the top or bottom flange (along the web). Concerning the support conditions, (i) the end sections are locally/globally pinned and can warp freely, and (ii) all in-plane cross-section displacements are fully restrained by the intermediate support.

While Table 2 compares the beam GBT and ANSYS critical loads corresponding to the two lengths and two loadings, Figs. 13(a)-(b) (*L=400cm*) and 14(a)-(b) (*L=800cm*) show the (i) ANSYS 3D views and (ii) GBT modal amplitude functions $\phi_k(x)$ concerning the associated buckling modes. After comparing these two sets of beam buckling results, the following comments are appropriate:

(i) The local deformation modes (**5**, **6**, **7**, **10**, **11**) have visible contributions to the *L=400cm* beam critical buckling modes shapes. While the instability of the beam loaded at the top flange is triggered by the localized web buckling occurring under the applied load, the buckling pattern of the beam loaded at the bottom flange is governed by the local deformation of the web and compressed flange taking place in the beam central region (around the intermediate support).

(ii) Although the *L=800cm* beam critical buckling is clearly lateral-torsional (predominant global modes **3**, **4**), there are also minor participations from the local deformation modes (**5**, **6**, **7**), particularly near

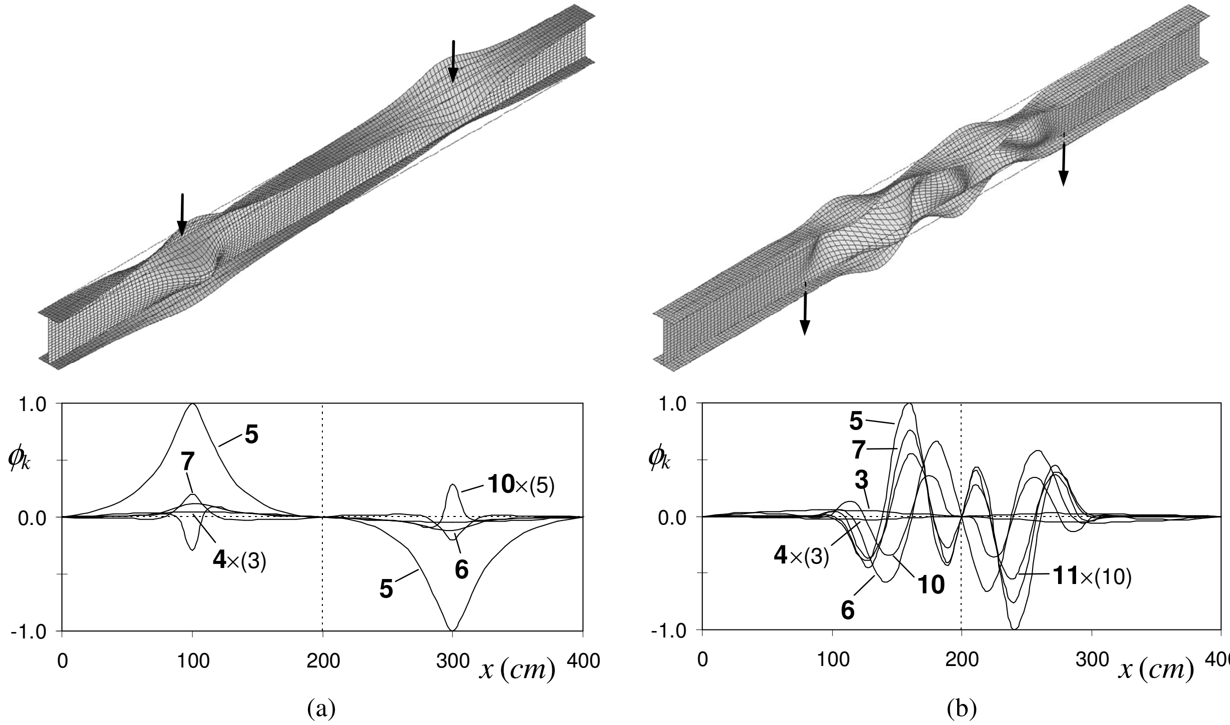

Figure 13: *L=400cm* two-span beam: ANSYS and GBT critical mode representations – (a) top and (b) bottom loading.

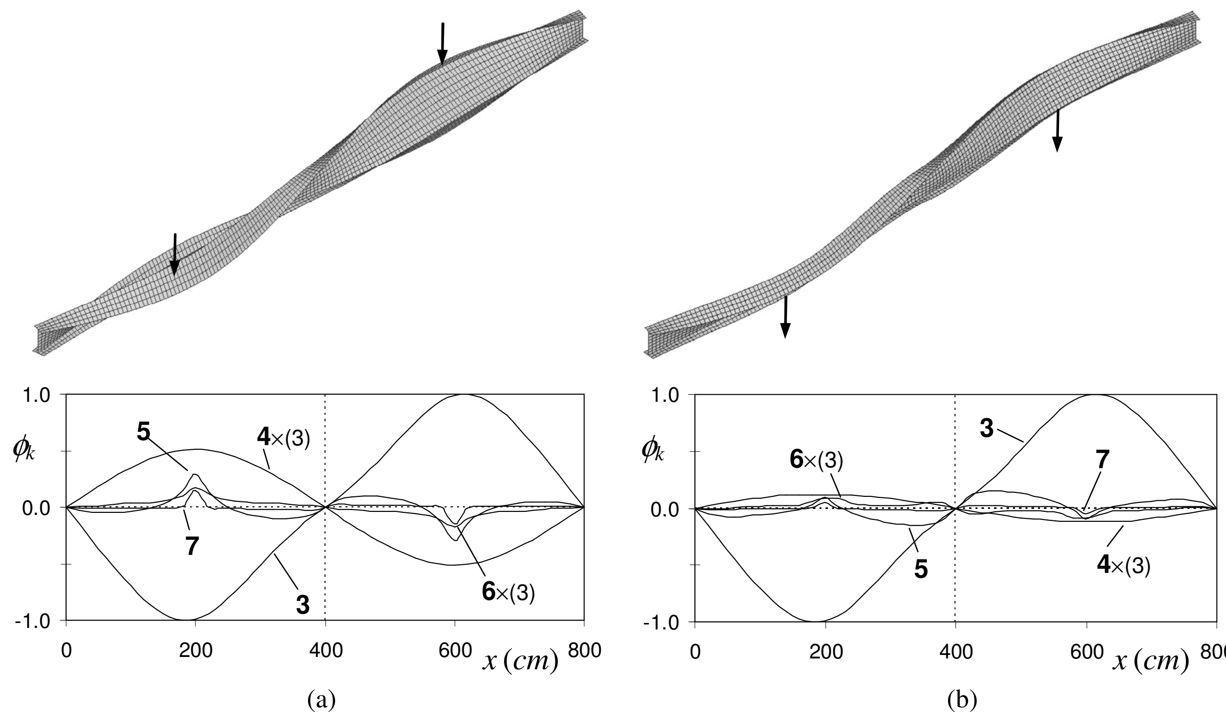

Figure 14: *L=800cm* two-span beam: ANSYS and GBT critical mode representations – (a) top and (b) bottom loading.

Table 2: GBT and ANSYS two-span beam critical load values (kN)

Length (cm)	*400*		*800*	
Load application	*Top*	*Bottom*	*Top*	*Bottom*
GBT	194.09	733.44	77.00	323.24
ANSYS	237.37	760.12	78.29	328.68
Δ (%)	-18.2	-3.5	1.6	-1.7

the loaded cross-sections. However, these local deformations are barely visible in the ANSYS 3D views and would certainly remain unnoticed without the GBT-based information.

(iii) From the critical buckling mode natures described in the previous two items, it is just logical to expect (iii_1) a close agreement between the GBT and ANSYS critical loads for the $L=400cm$ beam loaded at the bottom flange and the two $L=800cm$ beams, and (iii_2) a significant discrepancy for the $L=400cm$ beam loaded at the top flange. Indeed, the values presented in Table 2 fully confirm these expectations: while the differences concerning the three beams not experiencing web localized buckling are rather small (all under *3.5%*), there is a significant disparity in the remaining beam – the GBT critical buckling load underestimates its ANSYS counterpart by *18.2%*, due to the inadequate estimation of the geometric stiffness associated with the pre-buckling transverse normal stresses.

4.3 "L–frames"

Finally, two "L-frames" exhibiting the geometry, support conditions and loading shown in Fig. 15 are analyzed. They (i) are formed by equal-length ($L_c=L_b=600cm$) orthogonal members (column and beam) with I300×200 cross-sections, (ii) exhibit a box-stiffened joint (web continuity), (iii) are acted by a vertical point load P applied at the beam mid-span top or bottom flanges. In both frames, the column is laterally unrestrained and has a fully fixed end support, while the beam has a locally/globally pinned end support with free warping ("fork-type" support). The two frames differ in the fact that the beam is either laterally unrestrained or restrained by two intermediate supports, located at the web-flange corners of the $x_b=100cm$ cross-section (localised displacement restraints – see Fig. 15).

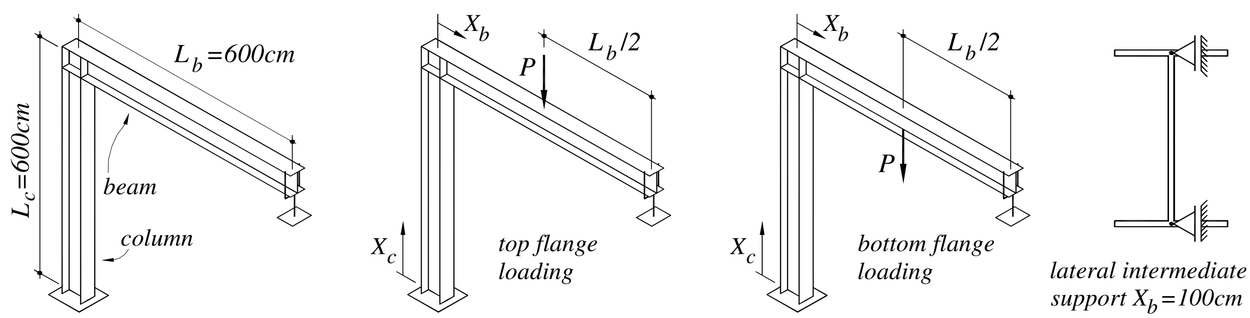

Figure 15: "L-shaped" frame geometry, support condition and loading.

Figs. 16(a)-(b) (unrestrained beam) and 17(a)-(b) (restrained beam), and Table 3, provide a comparison between the frame GBT and ANSYS critical buckling loads and modes concerning the two beam restraints and two loadings. The following conclusions can be drawn from the analysis of these buckling results:

(i) The influence of the load application effects on the critical buckling mode shape is more significant in the restrained frame. In the unrestrained frame, the critical buckling mode is predominantly lateral-torsional (modes **3**, **4**) for both loadings – the very small differences between the two mode shapes concern minor participations of local modes (**5**, **6**) near the loaded cross-section. In the restrained frame, on the other hand, the buckle mode switches from (ii_1) predominantly lateral-torsional, for top flange loading, to (ii$_2$) mostly local (modes **5**, **6**, **7**), with the deformation occurring in the beam mid-span region, for bottom flange loading – in both cases, the frame buckling is triggered by the beam instability.

(ii) Since none of the above frame critical buckling modes involves web localized instability, the GBT and ANSYS critical loads are expected to be quite close. Indeed, the values presented in Table 3 show that all differences are below *2.6%* (not surprisingly, the highest difference concerns the restrained frame loaded at the bottom flange – more local deformation near the loaded cross-section). Note also that there is very close agreement between the two critical buckling mode representations, even if the GBT modal amplitude functions provide more in-depth insight on the frame buckling mechanics.

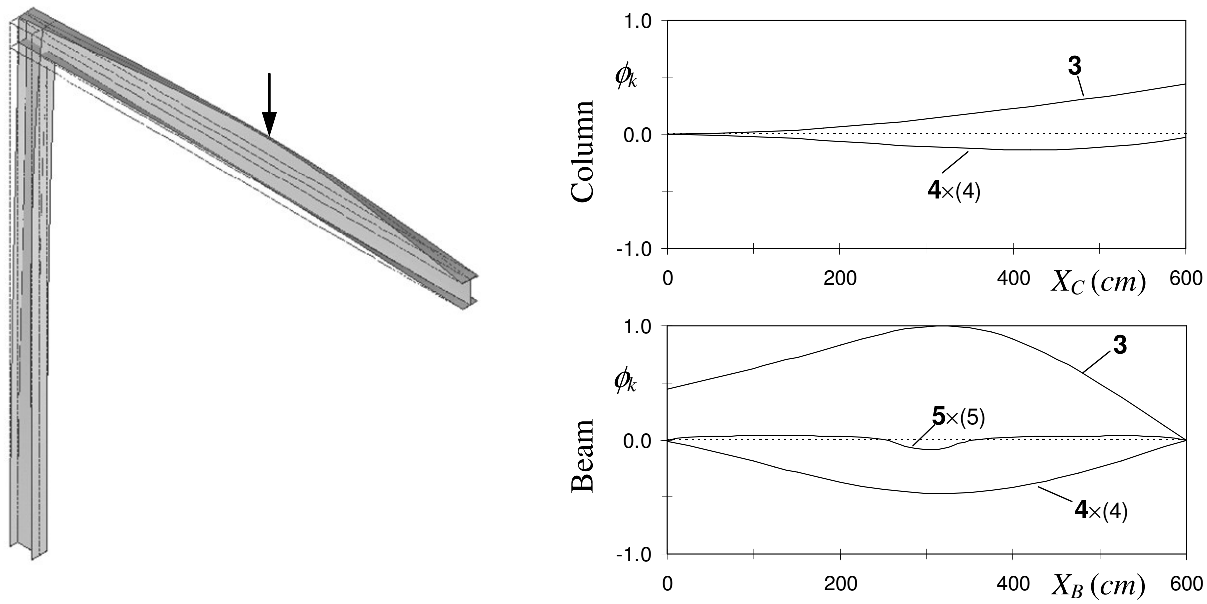

(a)

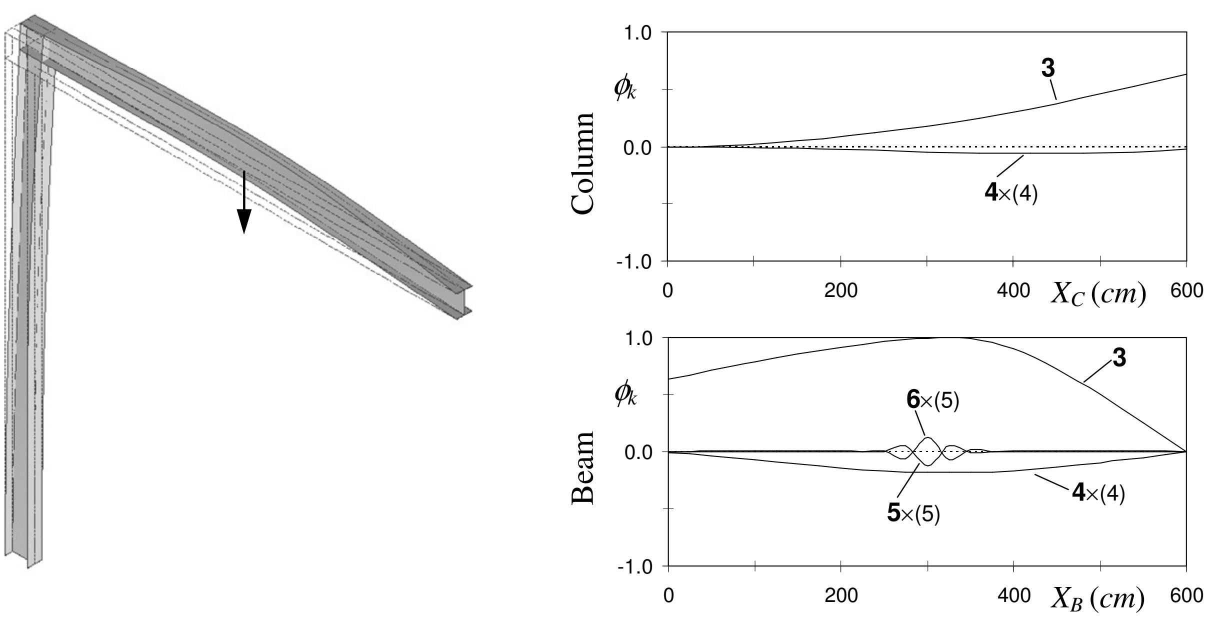

(b)

Figure 16: Unrestrained "L-shaped" frame: ANSYS and GBT critical mode representations – (a) top and (b) bottom loading.

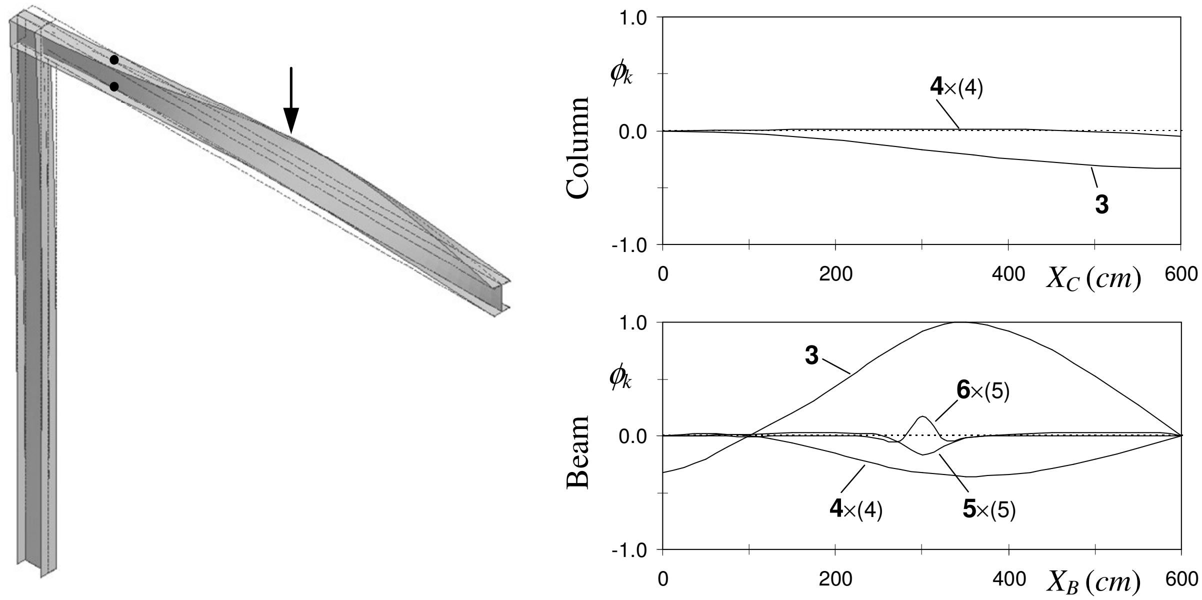

(a)

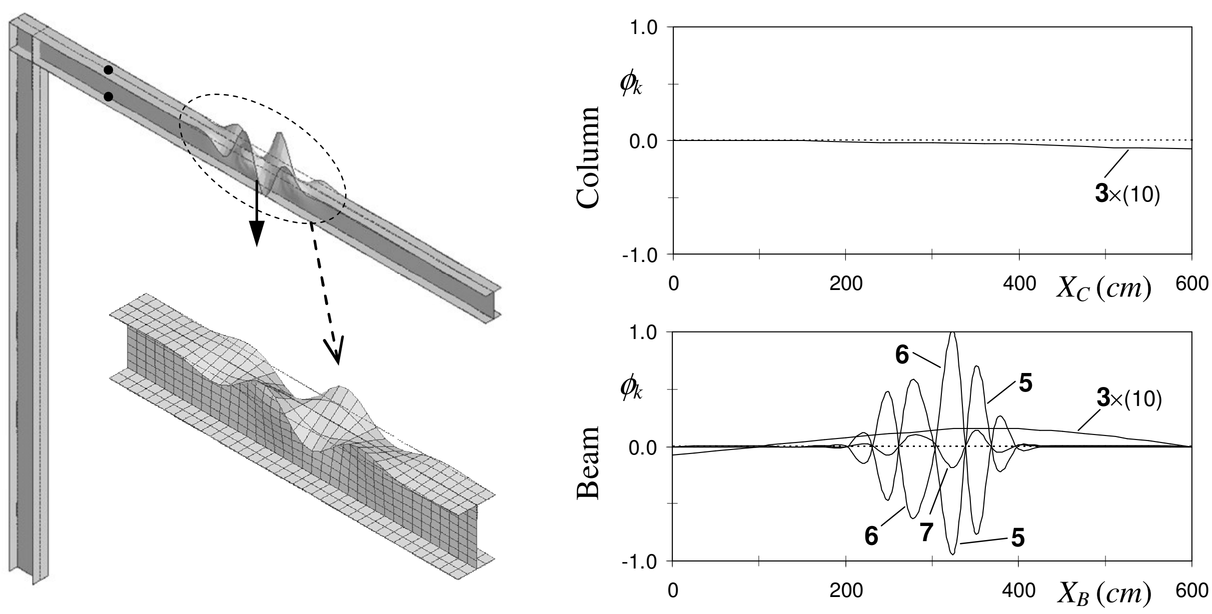

(b)

Figure 17: Restrained "L-shaped" frame: ANSYS and GBT critical mode representations – (a) top and (b) bottom loading.

Table 3: GBT and ANSYS frame critical load values (kN)

	Unrestrained		*Restrained*	
Load application	*Top*	*Bottom*	*Top*	*Bottom*
GBT	48.46	106.77	86.04	112.31
ANSYS	48.03	108.87	85.26	115.34
Δ (%)	0.8	-1.9	0.9	-2.6

(iii) The influence of the load application effects on the critical buckling load is higher in the unrestrained frame than in the restrained one – the differences are *120%* and *30%*, respectively.

5. Conclusion

This work addressed the development, finite element implementation and application of a GBT formulation to analyze the localized, local, distortional and global buckling behavior of thin-walled continuous beams and frames subjected to transverse loads applied at various member cross-section points (away from its shear centre) – *e.g.*, at the top and bottom flanges of I-section beams. The effects stemming from the transverse load position are accounted for through the incorporation of geometrical stiffness terms due to either (i) the internal work of the pre-buckling transversal normal stresses ("exact" formulation) or (ii) the external work of the applied transverse loads (approximate/simplified formulation).

Only the main concepts and procedures involved in the development of the "exact" formulation were presented – due to time limitations, its numerical implementation, which requires the performance of a rigorous GBT first-order analysis, and validation were not carried out in this work (they will be reported in the near future). Therefore, the numerical implementation and illustrations included in the paper concern only the approximate/simplified formulation, whose major limitation is related to the evaluation of the external work associated with the local deformation modes.

The illustrative numerical results presented and discussed involved (i) hat-section cantilevers, (ii) two-span I-section beams and (iii) "L-frames" built from I-section members, all acted by transverse loads applied at the top and bottom flanges. The accuracy of the GBT-based results was by means of the comparison with "exact" values, yielded by rigorous ANSYS shell finite element analyses. It was found that the proposed approximate/simplified formulation (i) always provides correct critical buckling mode shapes and (ii) leads to rather accurate critical buckling loads provided that no heavy web localized buckling is involved (*e.g.*, in web crippling problems). If this is the case, the beam finite element implementation of the "exact" formulation should (hopefully) produce similarly accurate critical loads.

Acknowledgments

The first author gratefully acknowledges the financial support of "*Fundação para a Ciência e Tecnologia*" (FCT – Portugal), through the post-doctoral scholarship nº SFRH/BPD/62904/2009.

References

Andrade A, Camotim D, Providência e Costa P. (2007). "On the evaluation of elastic critical moments in doubly and singly symmetric I-section cantilevers", *Journal of Constructional Steel Research*, **63**(7), 894-908.

Basaglia C, Camotim D, Silvestre N (2008). "GBT-based post-buckling analysis of thin-walled steel members and frames", *Proceedings of Structural Stability Research Council Annual Stability Conference* (SSRC 2008 – Nashville, 2-5/4), 215-237.

Basaglia C, Camotim D, Silvestre N (2010). "GBT-based buckling analysis of thin-walled steel frames with arbitrary loading and support conditions", *International Journal of Structural Stability and Dynamics*, **10**(3), 363-385.

Bebiano R, Silvestre N, Camotim D (2007). "GBT formulation to analyze the buckling behaviour of thin-walled members under non-uniform bending", *International Journal of Structural Stability and Dynamics*, **7**(1), 23-54.

Camotim D, Silvestre N, Basaglia C, Bebiano R (2008). "GBT-based buckling analysis of thin-walled members with non-standard support conditions", *Thin-Walled Structures*, **46**(7-9), 800-815.

Camotim D, Basaglia C, Silvestre N (2010a). "GBT buckling analysis of thin-walled steel frames: a state-of-the-art report", *Thin-Walled Structures*, **48**(10-11), 726-743.

Camotim D, Basaglia C, Bebiano R, Gonçalves R, Silvestre N (2010b). "Latest developments in the GBT analysis of thin-walled steel structures", *Proceedings of International Colloquium Stability and Ductility of Steel Structures* (SDSS'Rio 2010 – Rio de Janeiro, 8-10/9), E. Batista, P. Vellasco L. de Lima (Eds), 33-58.

Camotim D, Basaglia C, Silva NF, Silvestre N (2010c). "Numerical analysis of thin-walled structures using generalised beam theory (GBT): recent and future developments", *Computational Technology Reviews*, Vol. 1, B.H.V. Topping *et al.* (Eds.), Saxe-Coburg Publications, Stirlingshire, 315-354.

Gonçalves R (2007). *Analysis of Thin-Walled Beams with Deformable Cross-Sections: New Formulations and Applications*, PhD thesis in Civil Engineering, IST, Technical University of Lisbon. (Portuguese)

Gonçalves R, Dinis PB, Camotim D (2009). "GBT formulation to analyse the first-order and buckling behaviour of thin-walled members with arbitrary cross-sections", *Thin-Walled Structures*, **47**(5), 583-600.

Gonçalves R, Ritto-Corrêa M, Camotim D (2010). A new approach to the calculation of cross-section deformation modes in the framework of generalized beam theory", *Computational Mechanics*, **46**(5), 759-781.

Mohri F, Brouki A, Roth JC (2003). "Theoretical and numerical stability analyses of unrestrained, mono-symmetric thin-walled beams", *Journal of Constructional Steel Research*, **59**(1), 63-90.

Samanta A, Kumar A (2006). "Distortional buckling in monosymmetric I-beams", *Thin-Walled Structures*, **44**(1), 51-56.

SAS (Swanson Analysis Systems Inc.) (2009). *ANSYS Reference Manual* (version 12).

Schardt, R. (1989). *Verallgemeinerte Technische Biegetheorie*, Springer-Verlag, Berlin. (German)

Silva NF, Camotim D, Silvestre N (2008a). "Generalized Beam Theory formulation capable of capturing localized web buckling and load application effects", *Proceedings of 19th Specialty Conference on Cold-Formed Steel Structures* (St. Louis, 14-16/10), R. LaBoube, W.-W. Yu (eds.), 33-59.

Silva NF, Camotim D, Silvestre N (2008b). "GBT cross-section analysis of thin-walled members with arbitrary cross-sections: a novel approach", *Proceedings of Fifth International Conference on Thin-Walled Structures – Recent Innovations and Developments* (ICTWS 2008 – Brisbane, 18-20/6), M. Mahendran (Ed.), 1161-1171 (vol. 2).

Silva NF, Silvestre N, Camotim D (2010). "GBT formulation to analyse the buckling behaviour of FRP composite open-section thin-walled columns", *Composite Structures*, **93**(1), 79-92.

Silvestre N, Camotim D (2003a). "Non-linear generalised beam theory for cold-formed steel members", *International Journal of Structural Stability and Dynamics*, **3**(4), 461-490.

Silvestre N, Camotim D (2003b). "GBT buckling analysis of pultruded FRP lipped channel members", *Computers & Structures*, **81**(18-19), 1889-1904.

Trahair NS (1993). *Flexural-Torsional Buckling of Structures*, E & FN Spon (Chapman & Hall), London.

Wang CM, Kitipornchai S (1986). "Buckling capacities of monosymmetric I-beams", *Journal of Structural Engineering* (ASCE), **112**(11), 2372-2391.